Title

Magnetic resonance diffusion tensor imaging for the pedunculopontine nucleus: proof of concept and histological correlation

Journal

Brain Structure and Function, 222(6)

ISSN

1863-2653

Authors

Alho, ATDL
Hamani, C
Alho, EJL
et al.

Publication Date

2017-08-01

DOI

10.1007/s00429-016-1356-0

Peer reviewed

Published in final edited form as:

Brain Struct Funct. 2017 August ; 222(6): 2547–2558. doi:10.1007/s00429-016-1356-0.

Magnetic resonance diffusion tensor imaging for the pedunculopontine nucleus: proof of concept and histological correlation

A. T. D. L. Alho[1,2,3], **C. Hamani**[9], **E. J. L. Alho**[5], **R. E. da Silva**[2], **G. A. B. Santos**[2], **R. C. Neves**[3], **L. L. Carreira**[2], **C. M. M. Araújo**[2,3], **G. Magalhães**[1,2,3], **D. B. Coelho**[6], **M. C. Alegro**[1,2,8], **M. G. M. Martin**[2], **L. T. Grinberg**[3,4,8], **C. A. Pasqualucci**[3,4], **H. Heinsen**[2,3,7], **E. T. Fonoff**[5], and **E. Amaro Jr**[1,2]

[1]Hospital Israelita Albert Einstein, Instituto do Cérebro, São Paulo, Brazil

[2]Department of Radiology, Faculdade de Medicina da Universidade de São Paulo, Instituto de Radiologia, São Paulo, Brazil

[3]Grupo de Estudos em Envelhecimento Cerebral e LIM 22, Department of Pathology, Faculdade de Medicina da Universidade de São Paulo, São Paulo, Brazil

[4]Department of Pathology, Faculdade de Medicina da Universidade de São Paulo, São Paulo, Brazil

[5]Department of Neurology Faculdade de Medicina da Universidade de São Paulo, Divisão de Neurocirurgia Funcional do, Instituto de Psiquiatria-HCFMUSP, São Paulo, Brazil

[6]Escola de Educação Física e Esporte da Universidade de São Paulo, São Paulo, Brazil

[7]Department of Psychiatry, Psychiatric Clinic, Julius-Maximilians-University Würzburg, Universitätsklinikum Würzburg, Würzburg, Germany

[8]Memory and Aging Center, Department of Neurology, University of California, San Francisco, USA

[9]Division of Neurosurgery, Toronto Western Hospital, University of Toronto, Centre for Addiction and Mental Health, Toronto, Canada

Abstract

The pedunculopontine nucleus (PPN) has been proposed as target for deep brain stimulation (DBS) in patients with postural instability and gait disorders due to its involvement in muscle tonus adjustments and control of locomotion. However, it is a deep-seated brainstem nucleus without clear imaging or electrophysiological markers. Some studies suggested that diffusion tensor imaging (DTI) may help guiding electrode placement in the PPN by showing the surrounding fiber bundles, but none have provided a direct histological correlation. We investigated DTI fractional anisotropy (FA) maps from in vivo and in situ postmortem magnetic resonance images (MRI) compared to histological evaluations for improving PPN targeting in

Compliance with ethical standards

Conflict of interest The authors declare that there are no conflicts of interest.

humans. A post-mortem brain was scanned in a clinical 3T MR system in situ. Thereafter, the brain was processed with a special method ideally suited for cytoarchitectonic analyses. Also, nine volunteers had in vivo brain scanning using the same MRI protocol. Images from volunteers were compared to those obtained in the post-mortem study. FA values of the volunteers were obtained from PPN, inferior colliculus, cerebellar crossing fibers and medial lemniscus using histological data and atlas information. FA values in the PPN were significantly lower than in the surrounding white matter region and higher than in areas with predominantly gray matter. In Nissl-stained histologic sections, the PPN extended for more than 10 mm in the rostro-caudal axis being closely attached to the lateral parabrachial nucleus. Our DTI analyses and the spatial correlation with histological findings proposed a location for PPN that matched the position assigned to this nucleus in the literature. Coregistration of neuroimaging and cytoarchitectonic features can add value to help establishing functional architectonics of the PPN and facilitate neurosurgical targeting of this extended nucleus.

Keywords

Pedunculopontine nucleus; Deep brain stimulation; Diffusion tensor imaging; Histology

Introduction

The pedunculopontine nucleus (PPN) is a brainstem nucleus involved in the control of muscle tone and locomotion, both suggested to be abnormal in pathologies associated with gait and postural abnormalities (Hamani et al. 2007; Strauss et al. 2014). Besides locomotion, this nucleus also plays a role in mechanisms of sleep and cognitive function (Hazrati and Parent 1992; Kang and Kitai 1990; Saper and Loewy 1982).

The PPN has been proposed as a suitable target for deep brain stimulation (DBS) in patients with levodopa-resistant gait and postural disorders, including Parkinson disease (PD), atypical parkinsonian syndrome (APS) and progressive supranuclear palsy (PSP) (Benarroch 2013; Fraix et al. 2013; Zrinzo et al. 2008; de Oliveira Souza et al. 2016). Symptoms of advanced PD, such as freezing of gait and falls, respond poorly to dopaminergic treatment or surgical interventions in the subthalamic nucleus (STN) or globus pallidus internus (GPI)—the most commonly used DBS targets in PD. In a recent series of studies, PPN DBS has been shown to improve gait freezing and falls (Jenkinson et al. 2006; Thevathasan et al. 2011a, b; Ferraye et al. 2010; Fraix et al. 2013; Moro et al. 2010).

Success of DBS therapy depends on the precise targeting of the brain region of interest (Strauss et al. 2014). High field MRI sequences helped the precise implantation of DBS electrodes (Zrinzo et al. 2011). Unfortunately, the PPN and nearby structures cannot be clearly delineated with regular imaging sequences (Yelnik 2007; Zrinzo and Hariz 2007; Mazzone et al. 2016). To address this issue, Zrinzo et al. (2011) used a specific MRI-guided protocol (based on T1-weighted images) to target the human PPN in situ, followed by the confirmation of electrode placement with histological examination. Though the authors have used T1-weighted images and relied on indirect anatomical landmarks, no direct MR-based signal features were used in that study.

In most of its trajectory, the PPN lies posterior and lateral to the decussating superior cerebellar peduncle, medial to the medial lemniscus and lateral to the central tegmental tract (Fournier-Gosselin et al. 2013). As such, studies have suggested that DTI could help guiding electrode placement during PPN surgery (Muthusamy et al. 2007; Yeo et al. 2011). However, since the location of the PPN on imaging studies and histological sections has not been directly correlated, whether DTI can successfully contribute to localize the PPN in vivo remains unclear.

We investigated DTI and fractional anisotropy (FA) maps both in vivo and in post-mortem MR studies. In situ imaging findings were correlated with those obtained from actual histological sections of the same specimen.

Methods

The brain of a 66-year-old woman was obtained from the Brain Bank of the Brazilian Aging Brain Study Group (BBBABSG) of the Medical School-University of Sao Paulo (USP) and the Sao Paulo Autopsy Service (SPAS). Written informed consent was obtained from a family member. Premorbid clinical information was collected as previously described (Grinberg et al. 2007). Myocardial infarction was found to be the cause of death. No premorbid symptoms of cognitive decline or parkinsonism were detected (Ferretti et al. 2010).

As an in vivo control for post-mortem imaging and histological analyses, a group of nine subjects (three men and six women) without symptoms of cognitive decline or Parkinsonism underwent MRI scanning, as described below. All gave written informed consent. The study was approved by a local Ethics Committee (#09637112.2.0000.0065/Research Ethical Committee, Medical School—USP).

Magnetic resonance imaging acquisition

MR images of the post-mortem brain were acquired *before brain removal* in the Institute of Radiology-Hospital das Clínicas—USP within a 10-h post-mortem interval (PMI). Imaging data were acquired in a 3T MRI system (Achieva, Philips Medical Systems, Netherlands), equipped with an eight-channel head coil, and 80 mT/m gradients. DTI images were collected using a 2D-SENSE-GRE EPI-based acquisition: axial oblique slices oriented according to the AC-PC plane, slice thickness/gap: 2.0/0.0 mm, FOV: 256 × 256 mm, image matrix: 128 × 128 pixels (2.0 mm isotropic voxel size); TR: 23,650 ms, TE: 65 ms, b-value: 3000s/mm^2, gradient coding directions: 32, acceleration factor: 2.0, NEX: 2.0. FLAIR-weighted MR images were collected using 2D-FSE axial acquisition oriented according to AC-PC plane, slice thickness/gap: 3.0/0.3 mm, FOV:230 × 183 mm, image matrix 256 × 204 (voxel size: 3.0 × 0.9 × 0.9 mm), TR: 9686.7 ms, TI: 2800 ms, TE: 130 ms, NEX:1.0. The nine control volunteers and the postmortem brain were scanned using the same MR protocol (Table 1). The workflow is shown in Fig. 1.

Brain processing

Following autopsy, the brain was fixed in formalin 8%, dehydrated in a graded series of ethanol solutions and embedded in celloidin. The entire brain was serially sectioned on a

microtome (Polycut, Cambridge Instruments, UK). Axial, 430-μm-thick slices were then stained with Nissl staining and mounted as previously described by Heinsen et al. (2000) and Heinsen and Heinsen (1991). The complete workflow is described in Fig. 2.

MRI × histology registration, computer-assisted 3D reconstruction and target definition

Prior to cutting, the blockface of each section was photographed (Canon EOS 5D Mark II 21.1 Megapixel®, Tokyo, Japan). The distance between the camera and the blockface was kept constant throughout the process. Recorded images were stacked, aligned, and used for 3D reconstruction of the histological volume with the use of specialized software (Amira 5.3®, Mercury Systems). This software generated a surface based on individual outlines, which were manually traced on digital images (Heinsen et al. 2004; Di Lorenzo Alho et al. 2015).

Since histological processing causes tridimensional and bidimensional deformation (Quester and Schröder 1997; Schulz et al. 2011; Simmons and Swanson 2009), a computational coregistration of histological and in situ MR images was necessary. A pipeline was developed by our group (Alegro et al. 2015), which includes 2D and 3D registration, in three steps: (1) registering MRI, blockface and digitalized histology images; (2) bidimensional registration between histological images and blockface; (3) tridimensional registration between histological and MR images. Symmetric diffeomorphic registration method (SyN) (Avants et al. 2008) and ANTs (Avants et al. 2015) allows saving the transform that occurs during histological processing. Both can be reapplied in a segmented high-resolution mask (Fig. 3).

Pedunculopontine nucleus segmentation was performed in the original high-resolution digitalized histological images (dark and light field microscopy), allowing good contrast. Over those pictures, a mask was created with the original dimensions. Finally the registration transforms generated during processing were applied. This method allowed the PPN outlines to be accurately depicted in T1 MR images. The registration quality control was demonstrated in a previous work from our group (Alegro et al. 2015). To define the PPN stereotactic coordinates relative to the posterior comissure (PC) and Afshar's coordinate system (Afshar et al. 1978), we used SPM 12 (Neuroimaging Informatics Tools and Resources Clearinghouse, UCL, UK, 2014) to normalize the post-mortem MRI to the MNI space (ICBM152) and apply the transformations to our previously registered PPN masks.

Fractional anisotropy (FA) measure

FA values were obtained from volunteers, using manually traced oval regions of interest (ROI), based on the Olszewsky & Baxter Histological Atlas as well as on histological images obtained from the post-mortem serial brain sections (Fig. 3). Four ROIs were outlined: inferior colliculus (IC)(ROI area: 4.74mm^2), PPN region (PPN)(ROI area: 2.97mm^2), cerebellar crossing fibers (CCF) (ROI area: 5.05mm^2), and medial lemniscus (ML)(ROI area: 4.95mm^2) (Olszewski and Baxter 1982). These were chosen based on their topographical relationship with the PPN. ROIs were traced in four consecutive slides using FA maps and FLAIR using the Osirix software (v.4.1—Pixmeo, Geneva, Swiss). FA values

were obtained in post-mortem and in vivo datasets of the right and left hemi-brainstem for each slice.

Statistical analysis

ANOVA (Tukey post hoc) was used to analyze six comparisons per family (Alpha 0.05, 95% confidence interval) and compare FA values in each ROI across different volunteers.

Results

Locating PPN by comparing FLAIR-weighted MRI with stereotactic atlases

In this study, we chose to use the Olszewski and Baxter atlas as a reference to localize the PPN (Olszewski and Baxter 1982). In that publication, the PPN is described as a nucleus with ascending and descending connections represented at the level of the inferior colliculi (IC) and the mesencephalic aqueduct (AQ). The nucleus lies medial to the lemniscal system (LS) and lateral to cerebellar crossing fibers (CCF) (Fig. 3a–c). The inferior pole of the PPN is close to superior aspect of the locus coeruleus (LC). On image studies, the PPN has been described as a gray matter area situated in the middle of white matter fiber tracts (Fig. 4).

The initial step in our study was to compare the location of the PPN region on FLAIR images, atlas plates and histological slides. In all modalities, the superior border of the nucleus was found at the level of the IC and AQ with its inferior pole located near the superior pole of LC, approximately 3–4 mm medial to the lateral edge of the brainstem (Fig. 4).

These images helped to determine the ROIs in FA colored maps. Between the ML and CCF fiber bundles, we identified a dark region in each side of the brainstem possibly representing the gray matter area where the PPN and other nuclei could be located (Fig. 3e). This proposed PPN location matches the position the nucleus as observed in atlas plates and FLAIR-weighted MRI images.

Measuring and comparing FA values

We have observed that the FA values in adjacent brain stem structures were found quite diverse. In the PPN region (0.67 ± 0.10) FA values were found intermediate when compared to the surrounding white matter corresponding to the ML (0.82 ± 0.06) and CCF (0.77 ± 0.06) and to the gray matter of the IC (0.61 ± 0.10) (ANOVA-Friedman test $P < 0.0001$) (see Fig. 5). These findings may suggest that the region where the PPN is located is composed by predominantly gray matter rich in myelinated fibers. Those findings are in accordance to the cytoarchitectonic description of the PPN as a nucleus with abundant ascending and descending connections.

Locating PPN by comparing human brain histological and imaging analysis

In our Nissl-stained sections, the PPN extended for more than 10 mm in the rostro-caudal axis. Its caudal part could be identified at rostral level of locus coeruleus (LC). Here, it was closely related to the lateral parabrachial nucleus (PBL). The PPN reveals a sickle shape in axial planes up to the caudal levels of the substantia nigra (SN), after which its rostral half

becomes triangular at the caudal plane of the trochlear nucleus (IV). Its rostral end was closely opposed to the dopaminergic ventral tegmental area A10, or cell groups of the parabrachial pigmented nucleus (PBB) at the level of the posterior part of red nucleus. The compact sub-nucleus could be identified in central four-fifths of the PPN. Overall, we verified that the dark field image compared to MRI corresponds to the gray area surrounding the fiber system around the gray matter region where PPN is likely to be located (Fig. 3e).

In summary, data from histological slides matched the PPN location observed in FLAIR-weighted MRI imaging and DTI. A tridimensional reconstruction of the human brain analyzed herein represents the PPN as a purple nucleus between the ML and CCF in a region located in between the SN below and red nucleus (RN) above (Figs. 4, 6, 7, 8, 9, 10).

PPN stereotactic coordinates

As described above, the location of the PPN in our study was initially defined based on atlas plates derived and our histological slides. The latter were segmented in high-resolution histological images (dark and light field microscopy) and transferred to stereotactic MR space. Stereotactic coordinates of the PPN centroid relative to PC and Afshar's coordinate system (Afshar et al. 1978) are shown in Table 2 and Figs. 6, 7, 8, 9, 10.

Discussion

The precise location of the human PPN on imaging studies has gained increased attention because of its involvement in motor diseases (Fraix et al. 2013; Zrinzo et al. 2011, 2008; Mazzone et al. 2007). Except for the study by Zrinzo et al. (2011) other reports have largely failed to validate the proposed histological location of the PPN (Zrinzo et al. 2011). In their study, however, Zrinzo and colleagues (2011) have used conventional T1 MRI, which does not precisely define anatomical aspects of small brain structures. As the PPN is surrounded by fiber-rich structures, we have decided to investigate FA measures obtained from both in vivo and in post-mortem MRI.

We determined the PPN location and nearby fiber tracts in histological sections, matching the description of Olszewski & Baxter (1982) and after normalizing the data to a common stereotactic space (MNI-ICBM 152), coordinates of the histological nucleus were transported to the MRI of control live subjects in order to analyze the FA maps of the region. The area in which the PPN is located has a distinct low signal on FA maps extending between the LS and CCF fiber bundles in the medial–lateral axis and the IC and LC in the dorsal ventral axis (Fig. 3) (Yeo et al. 2011; Zrinzo et al. 2011). This imaging-derived PPN site was confirmed in both post-mortem and in vivo datasets and corroborated the location of the PPN observed in histological sections (Fig. 3). The location of the PPN, as indicated by our DTI analyses, also corroborates that suggested by previous MR-based analyses (Hamani et al. 2011; Zrinzo et al. 2011). The PPN extended for over 10 mm in the longitudinal axis of the brainstem, lying in the vicinity of the lateral parabrachial nucleus.

The first study using PPN stimulation to treat movement disorders reported an acute improvement in postural stability and gait in PD patients (Plaha and Gill 2005). After this original endeavor, therapeutic results of PPN stimulation were contradictory (Hamani et al.

2011). For instance, while one report showed that PPN stimulation improved PD-related falls, another questioned the efficacy of the PPN DBS since either PD subjects did not respond or had a worsening on posture and stability (Moro et al. 2010; Ferraye et al. 2010). Conflicting results such as the ones described above led to much discussion as to whether discrepancies could be due to an inaccurate positioning of the electrodes or if the PPN is actually best target for treating gait symptoms in PD and related disorders. By the time PPN drew attention as a potential therapeutic target, the topographical position of the nucleus in the brain stem was not clear in the literature. Stereotactic surgeons faced a problem; neither MR image protocols nor electrophysiological markers helped sufficiently the targeting of the PPN. Besides that, the PPN location and its borders were not precisely defined in the textbooks and available brain atlases. Additionally, different nomenclatures were used to identify the region of the PPN in different Atlases. The Atlas of Schaltenbrand and Warren, one of the most used atlases to guide functional and stereotactic procedures, refers to the region of the pedunculopontine nucleus as Tg.pdpo (nucleus tegumenti pedunculo-pontinus). This has lead to some confusion in important publications that used different areas such as the Ppd (nucleus peripeduncularis) as being the PPN (Stefani et al. 2007; Yelnik 2007). The aim of the present study was to provide a reproducible and individual-based image method that may be used as an image marker facilitating its targeting of the PPN based in the contrast of the FA values of gray and surrounding white matter in this region. A novel aspect in our study, but also an important step to demonstrate the robustness of the method was to provide the possibility to check the coregistration of neuroimaging of the PPN region with the corresponding histological data. With this approach, we could establish a combination of MRI methods to better visualize brainstem structures of interest. These included T2 and FLAIR-weighted acquisitions with a good contrast and resolution combined with FA maps. On the other hand, we could also observe how inaccurate is to find the location of PPN using only stereotactic coordinates based on indirect methods (i.e., relative to AC, PC and the ventricular floor line). This can be even worse if there is significant hemispheric asymmetry. In this particular case, neuroimaging studies were corroborated by histological analyses in showing asymmetric location of the PPN. In fact, this is in line with previous findings suggesting natural asymmetries in subcortical and brainstem nuclei in different hemispheres (Mazzone et al. 2008; Fournier-Gosselin et al. 2013). It is urgent to develop more reliable methods to directly target and visualize the PPN using other neuroimaging modalities. Particularly in this case, DTI/FA sequence was found more important than T2 and Flair. We note, however, that resolution using our FA map was not sufficient to delineate small brainstem nuclei. Subdivisions with the gray matter and small nuclei adjacent to PPN such as cuneiform and subcuneiform nuclei could not be identified. We hope that by increasing the resolution and the quality of MR images using 7T MRI these nuclei may be distinguished in the future.

Indeed histological analysis shows that the PPN is narrow and elongated island of gray matter surrounded by fibers *en passage* from different systems (Fig. 4). It is also extremely permeated by fibers connecting the PPN with numerous cranial and caudal structures in the neuroaxis (Fournier-Gosselin et al. 2013). This is corroborated by the present results, showing that the PPN holds an intermediate FA values when compared to the fiber bundles (high FA values) and to the inferior colliculus (low FA values). So far, electrical stimulation

has been delivered in the PPN through cylindrical omnidirectional electrodes that generates a spherical or oval-shaped electrical field. Considering the anatomy of this area, it is likely that a considerable part of the tissue influenced by the electrical field is constituted by the surrounding fibers, so it is reasonable to infer that, at least part of the clinical results of the PPN-DBS is related to fiber bundle stimulation. Future studies may benefit from electrodes able to provide complex-shaped electrical fields to directionally orient more selective stimulation. This new technology may offer valuable data considering the correlation between selective stimulation and clinical effects. This may lead us to a better understanding the function of different tracts in specific neurological conditions.

In conclusion, our study contributes to the literature by showing, for the first time, the neuroanatomical landmarks of the PPN region as observed in particular MR sequences with the corresponding histological data of the same brain. We conclude that the PPN region may be best visualized on neuroimaging studies if specific sets of MRI/DTI parameters/sequences are used. Though promising, whether our approach will be useful to help targeting the PPN during DBS surgery still needs to be demonstrated in clinical practice. We believe that, the method of merging high-quality histological MR images can facilitate the localization of deep brain structures for clinical use and further refine the stereotactic targeting.

Acknowledgments

We are grateful to the volunteers who participated and family members who donated the brain for this study. We would also like to thank all the members of the Brain Bank of the Brazilian Aging Brain Study Group. Funding sources: Brazilian National Council for Scientific and Technological Development (CNPq), Institute for Education and Research of Albert Einstein Hospital, São Paulo Research Foundation (FAPESP), LIM-22 and LIM-44 (HC-FMUSP) for research financial and technical support in Brazil, and the National Institutes of Health, USA (R01AG040311).

Funding Brazilian National Council for Scientific and Technological Development (CNPq), Institute for Education and Research of Albert Einstein Hospital, São Paulo Research Foundation (FAPESP), LIM-44 and LIM-22 (HC-FMUSP) for research financial and technical support in Brazil, and the National Institutes of Health, USA (R01AG040311).

References

Afshar, F., Watkins, ES., Yap, JC. Stereotaxic atlas of the human brainstem and cerebellar nuclei: a variability study. Raven Press; New York: 1978.

Alegro, M., Alho, EJL., Lopes, R., Zollei, L., Amaro-Junior, E. A Computational Pipeline for Full Brain Histology to MRI registration. Organization for Human Brain Mapping; Honolulu, Hawaii, USA: 2015.

Avants BB, Epstein CL, Grossman M, Gee JC. Symmetric diffeomorphic image registration with cross-correlation: evaluating automated labeling of elderly and neurodegenerative. Brain. 2008; 12(1):26–41.

Avants, BB., Tustison, N., Song, G. Advanced normalization tools (stnava.github.io/ants). USA: 2015.

Benarroch EE. Pedunculopontine nucleus: functional organization and clinical implications. Neurology. 2013; 80(12):1148–1155. [PubMed: 23509047]

de Oliveira Souza C, de Lima-Pardini AC, Coelho DB, Brant R, Lopes-Alho EJ, Di Lorenzo-Alho AT, Teixeira LA, Teixeira MJ, Barbosa ER, Fonoff ET. Pedunculopontine DBS improves balance in progressive supranuclear palsy: instrumental analysis. Clin Neurophys. 2016; In press. doi: 10.1016/j.clinph.2016.09.006

Di Lorenzo Alho AT, Suemoto CK, Polichiso L, Tampellini E, de Oliveira KC, Molina M, Santos GA, Nascimento C, Leite RE, de Lucena Ferreti-Rebustini RE, da Silva AV, Nitrini R, Pasqualucci CA, Jacob-Filho W, Heinsen H, Grinberg LT. Three-dimensional and stereological characterization of the human substantia nigra during aging. Brain Struct Funct. 2015; doi: 10.1007/s00429-015-1108-6

Ferraye MU, Debû B, Fraix V, Goetz L, Ardouin C, Yelnik J, Henry-Lagrange C, Seigneuret E, Piallat B, Krack P, Le Bas JF, Benabid AL, Chabardès S, Pollak P. Effects of pedunculopontine nucleus area stimulation on gait disorders in Parkinson's disease. Brain. 2010; 133:205–214. [PubMed: 19773356]

Ferretti, REdL, Damin, AE., Brucki, SMD., Morillo, LS., Perroco, TR., Campora, F., Moreira, EG., Balbino, ÉS., Lima, MdCdA, Batella, C., Ruiz, L., Grinberg, LT., Farfel, JM., Leite, REP., Suemoto, CK., Pasqualucci, CA., Rosemberg, SR., Saldiva, PHN., Jacob-Filho, W., Nitrini, R. Post-mortem diagnosis of dementia by informant interview. Dement Neuropsychol. 2010; 4(2):6.

Fournier-Gosselin MP, Lipsman N, Saint-Cyr JA, Hamani C, Lozano AM. Regional anatomy of the pedunculopontine nucleus: relevance for deep brain stimulation. Mov Disord. 2013; 28(10):1330–1336. [PubMed: 23926071]

Fraix V, Bastin J, David O, Goetz L, Ferraye M, Benabid AL, Chabardes S, Pollak P, Debû B. Pedunculopontine nucleus area oscillations during stance, stepping and freezing in Parkinson's disease. PLoS One. 2013; 8(12):e83919. [PubMed: 24386308]

Grinberg LT, Ferretti RE, Farfel JM, Leite R, Pasqualucci CA, Rosemberg S, Nitrini R, Saldiva PH, Filho WJ, Group BABS. Brain bank of the Brazilian aging brain study group—a milestone reached and more than 1,600 collected brains. Cell Tissue Bank. 2007; 8(2):151–162. [PubMed: 17075689]

Hamani C, Stone S, Laxton A, Lozano AM. The pedunculopontine nucleus and movement disorders: anatomy and the role for deep brain stimulation. Parkinsonism Relat Disord. 2007; 13(Suppl 3):S276–S280. [PubMed: 18267250]

Hamani C, Moro E, Lozano AM. The pedunculopontine nucleus as a target for deep brain stimulation. J Neural Transm. 2011; 118(10):1461–1468. [PubMed: 21194002]

Hazrati LN, Parent A. Projection from the deep cerebellar nuclei to the pedunculopontine nucleus in the squirrel monkey. Brain Res. 1992; 585(1–2):267–271. [PubMed: 1380869]

Heinsen H, Heinsen YL. Serial thick, frozen, gallocyanin stained sections of human central nervous system. J Histotechnol. 1991; 14(3):7.

Heinsen H, Arzberger T, Schmitz C. Celloidin mounting (embedding without infiltration)—a new, simple and reliable method for producing serial sections of high thickness through complete human brains and its application to stereological and immunohistochemical investigations. J Chem Neuroanat. 2000; 20(1):49–59. [PubMed: 11074343]

Heinsen H, Arzberger T, Roggendorf W, Mitrovic T. 3D reconstruction of celloidin-mounted serial sections. Acta Neuropathologica. 2004; 108:374.

Jenkinson N, Nandi D, Oram R, Stein JF, Aziz TZ. Pedunculopontine nucleus electric stimulation alleviates akinesia independently of dopaminergic mechanisms. Neuroreport. 2006; 17(6):639–641. [PubMed: 16603926]

Kang Y, Kitai ST. Electrophysiological properties of pedunculopontine neurons and their postsynaptic responses following stimulation of substantia nigra reticulata. Brain Res. 1990; 535(1):79–95. [PubMed: 2292031]

Mazzone P, Insola A, Lozano A, Galati S, Scarnati E, Peppe A, Stanzione P, Stefani A. Peripeduncular and pedunculopontine nuclei: a dispute on a clinically relevant target. Neuroreport. 2007; 18(13): 1407–1408. [PubMed: 17762723]

Mazzone P, Sposato S, Insola A, Dilazzaro V, Scarnati E. Stereotactic surgery of nucleus tegmenti pedunculopontine [corrected]. Br J Neurosurg. 2008; 22(Suppl 1):S33–40. [PubMed: 19085351]

Mazzone P, Garcia-Rill E, Scarnati E. Progress in deep brain stimulation of the pedunculopontine nucleus and other structures: implications for motor and non-motor disorders. J Neural Transm (Vienna). 2016; doi: 10.1007/s00702-016-1532-7

Moro E, Hamani C, Poon YY, Al-Khairallah T, Dostrovsky JO, Hutchison WD, Lozano AM. Unilateral pedunculopontine stimulation improves falls in Parkinson's disease. Brain. 2010; 133:215–224. [PubMed: 19846583]

Muthusamy KA, Aravamuthan BR, Kringelbach ML, Jenkinson N, Voets NL, Johansen-Berg H, Stein JF, Aziz TZ. Connectivity of the human pedunculopontine nucleus region and diffusion tensor imaging in surgical targeting. J Neurosurg. 2007; 107(4):814–820. [PubMed: 17937229]

Olszewski, J., Baxter, D. Cytoarchitecture of the Human Brain Stem. Karger; Basel, Switzerland: 1982.

Plaha P, Gill SS. Bilateral deep brain stimulation of the pedunculopontine nucleus for Parkinson's disease. Neuroreport. 2005; 16(17):1883–1887. [PubMed: 16272872]

Quester R, Schröder R. The shrinkage of the human brain stem during formalin fixation and embedding in paraffin. J Neurosci Methods. 1997; 75(1):81–89. [PubMed: 9262148]

Saper CB, Loewy AD. Projections of the pedunculopontine tegmental nucleus in the rat: evidence for additional extrapyramidal circuitry. Brain Res. 1982; 252(2):367–372. [PubMed: 7150958]

Schulz G, Crooijmans HJ, Germann M, Scheffler K, Müller-Gerbl M, Müller B. Three-dimensional strain fields in human brain resulting from formalin fixation. J Neurosci Methods. 2011; 202(1): 17–27. [PubMed: 21889536]

Simmons DM, Swanson LW. Comparing histological data from different brains: sources of error and strategies for minimizing them. Brain Res Rev. 2009; 60(2):349–367. [PubMed: 19248810]

Stefani A, Lozano AM, Peppe A, Stanzione P, Galati S, Tropepi D, Pierantozzi M, Brusa L, Scarnati E, Mazzone P. Bilateral deep brain stimulation of the pedunculopontine and subthalamic nuclei in severe Parkinson's disease. Brain. 2007; 2007130(6):1596–1607.

Strauss I, Kalia SK, Lozano AM. Where are we with surgical therapies for Parkinson's disease? Parkinsonism Relat Disord. 2014; 20(Suppl 1):S187–S191. [PubMed: 24262178]

Thevathasan W, Coyne TJ, Hyam JA, Kerr G, Jenkinson N, Aziz TZ, Silburn PA. Pedunculopontine nucleus stimulation improves gait freezing in Parkinson disease. Neurosurgery. 2011a; 69(6): 1248–1253. (discussion 1254). [PubMed: 21725254]

Thevathasan W, Pogosyan A, Hyam JA, Jenkinson N, Bogdanovic M, Coyne TJ, Silburn PA, Aziz TZ, Brown P. A block to pre-prepared movement in gait freezing, relieved by pedunculopontine nucleus stimulation. Brain. 2011b; 134:2085–2095. [PubMed: 21705424]

Yelnik J. PPN or PPD, what is the target for deep brain stimulation in Parkinson's disease? Brain. 2007; 130:e79. (author reply e80). [PubMed: 17586558]

Yeo SS, Kim SH, Ahn YH, Son SM, Jang SH. Anatomical location of the pedunculopontine nucleus in the human brain: diffusion tensor imaging study. Stereotact Funct Neurosurg. 2011; 89(3):152–156. [PubMed: 21494066]

Zrinzo L, Hariz M. The peripeduncular nucleus: a novel target for deep brain stimulation? Neuroreport. 2007; 18(15):1631–1632. (author reply 1632–1633). [PubMed: 17948606]

Zrinzo L, Zrinzo LV, Tisch S, Limousin PD, Yousry TA, Afshar F, Hariz MI. Stereotactic localization of the human pedunculopontine nucleus: atlas-based coordinates and validation of a magnetic resonance imaging protocol for direct localization. Brain. 2008; 131(Pt 6):1588–1598. [PubMed: 18467343]

Zrinzo L, Zrinzo LV, Massey LA, Thornton J, Parkes HG, White M, Yousry TA, Strand C, Revesz T, Limousin P, Hariz MI, Holton JL. Targeting of the pedunculopontine nucleus by an MRI-guided approach: a cadaver study. J Neural Transm. 2011; 118(10):1487–1495. [PubMed: 21484277]

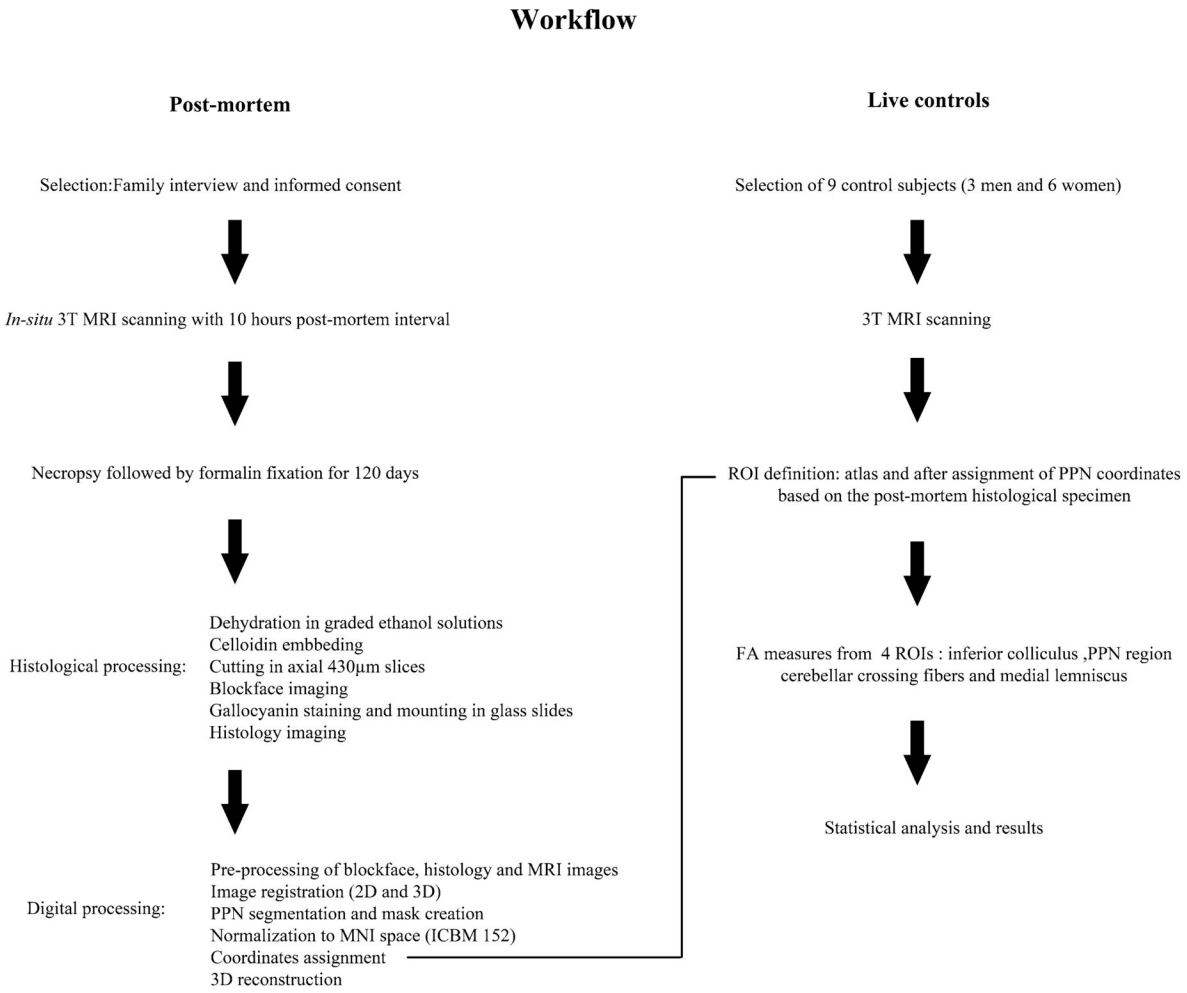

Fig. 1.
Workflow of post-mortem and live controls data management

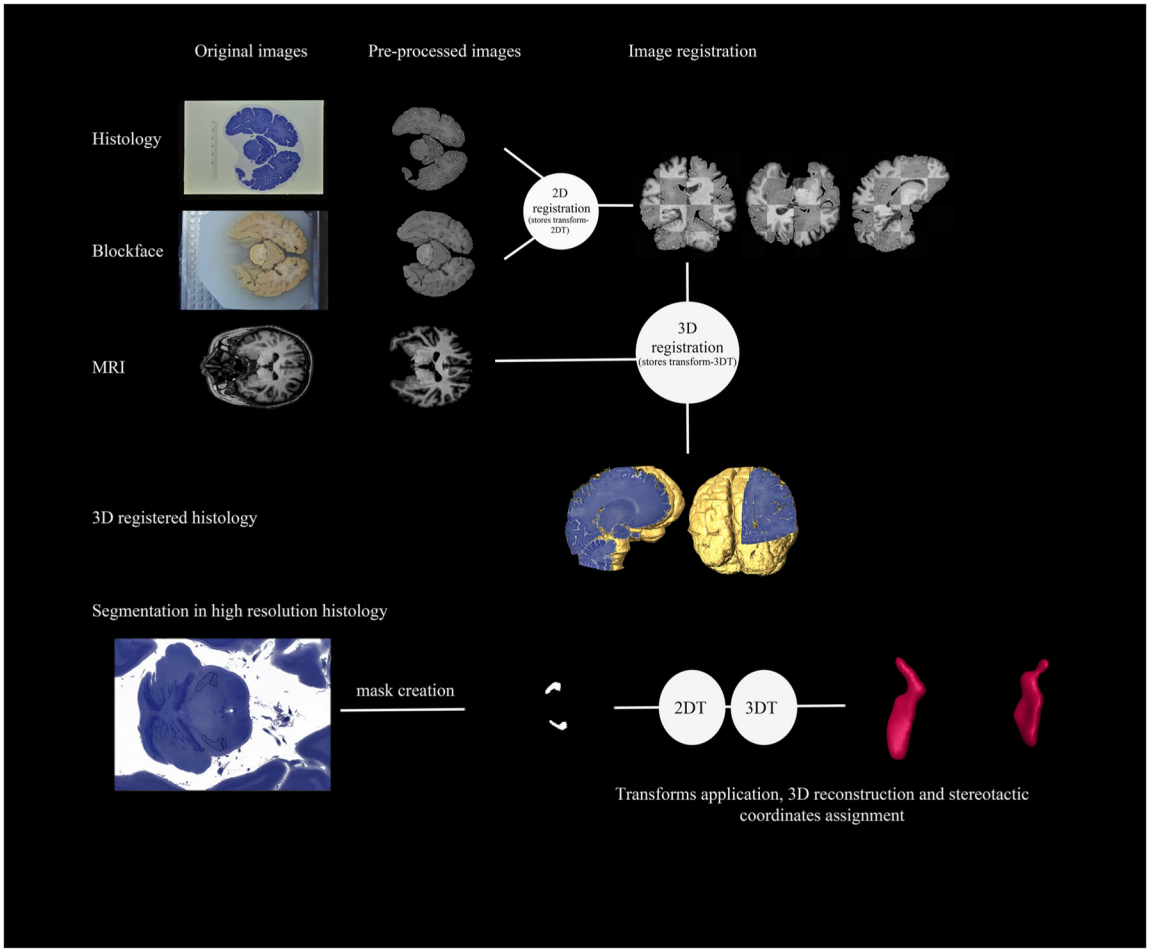

Fig. 2.

Workflow of the digital processing of the post-mortem specimen: magnetic resonance images, high field histological images and block-face pictures

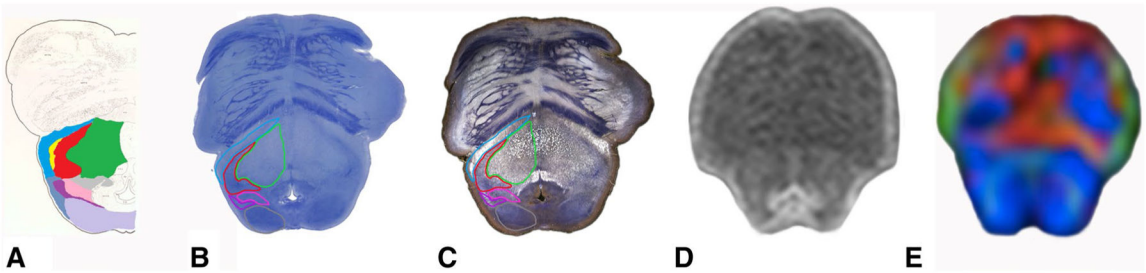

Fig. 3.

a Olszewsky & Baxter Histological Atlas showing brainstem nuclei at the level of the pons: locus coeruleus (*gray*); nucleus cuneiformis (*pink*); PPN (*red*) nucleus parabrachialis lateralis *(yellow)*; inferior colliculus *(light purple*); nucleus sagulum (*dark blue*); medial lemniscus (*light blue*); lateral lemniscus *(dark purple)* and cerebellar crossing fibers (*green*). Pictures of the brainstem in lightfield (**b**) and darkfield (**c**), axial flair (**d**) and FA colored map (**e**)

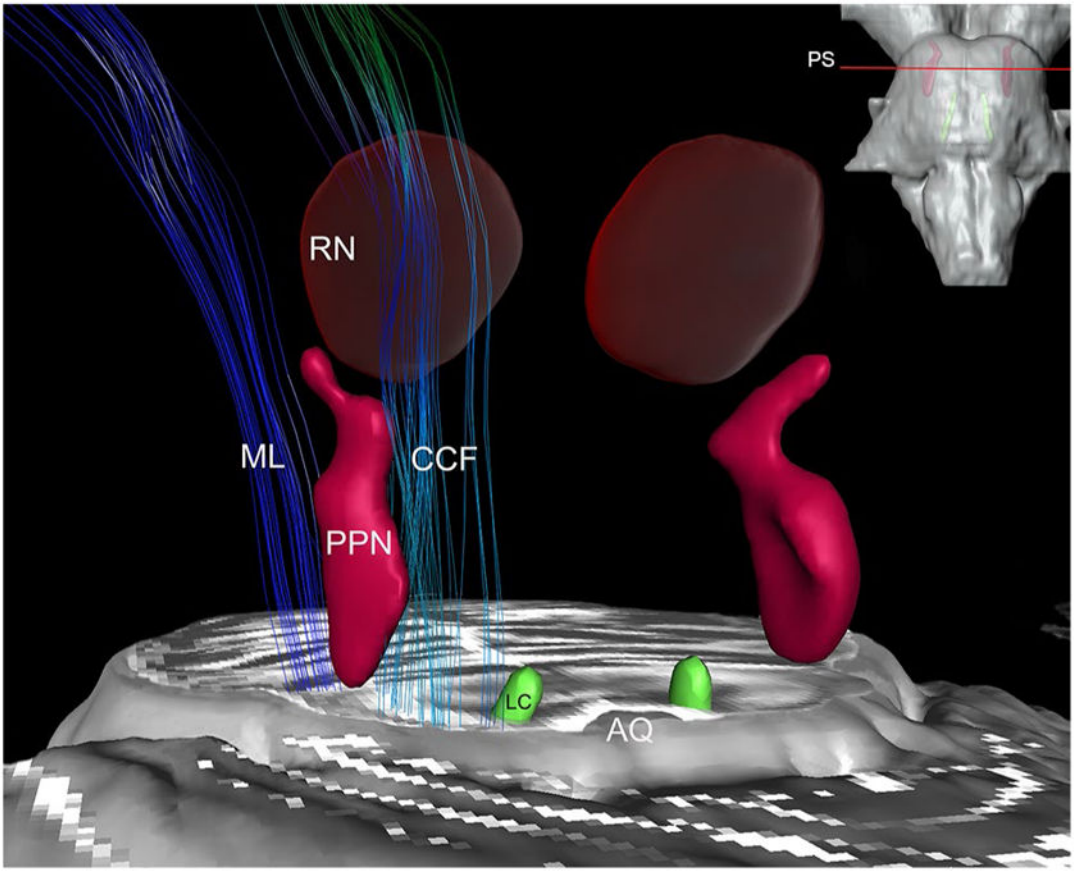

Fig. 4.

3D reconstruction of the PPN, red nucleus (RN), *locus coeruleus* (LC), aqueduct (AQ), medial lemniscus fibers (ML) and cerebellar crossing fibers (CCF) passing around the nuclei. On the *bottom right side*, the brainstem indicating the plane of section (PS)

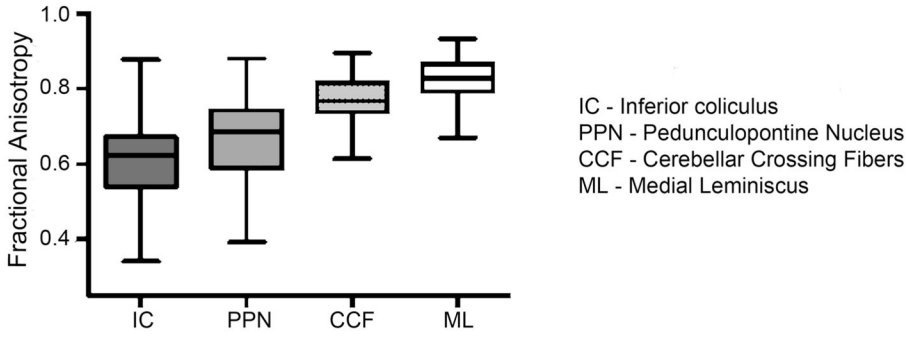

Fig. 5.

Comparison between FA values of the inferior colliculus (IC), pedunculopontine nucleus (PPN), cerebellar crossing fibers (CCF) and medial lemniscus (ML): mean FA values: IC = 0.61; PPN = 0.67; CCF = 0.77; ML = 0.82

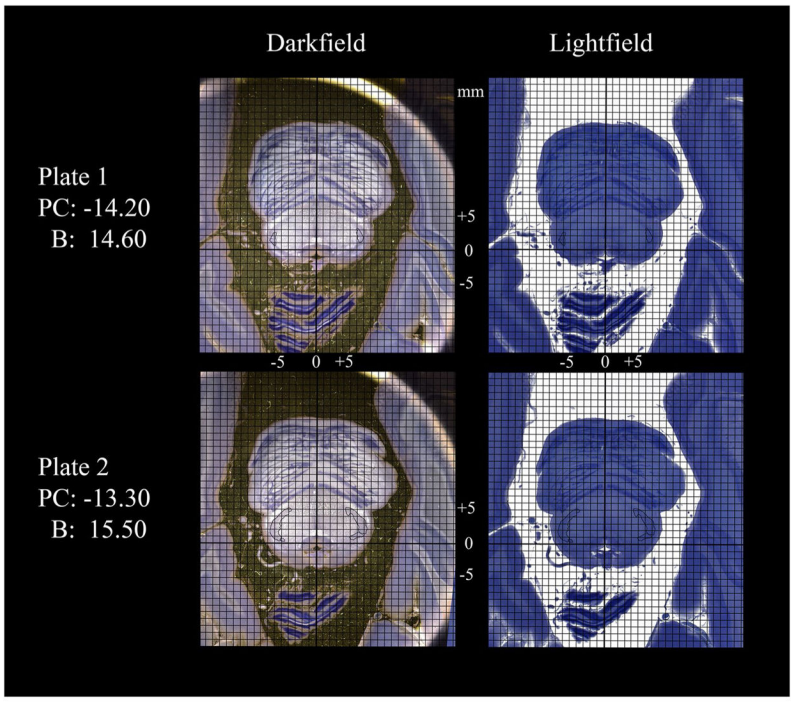

Fig. 6.

Plates 1–2 representing brainstem with pedunculopontine area. Nissl-stained (430 μm *thick*) showing dark and light field microscopy, and the mask with PPN region. The histological set of images was oriented in the axial plane, parallel to h1 and the B–F line, as defined by Afshar (Afshar et al. 1978). The h1 line emerges in an acute angle (15°) at the crossing point of the projection of the AC-PC line and the projection of the ventricular floor line (VLF) and runs in a rostral direction. Stereotactic coordinates of the PPN before registration to MRI are given relatively to this system, as considered to be more reliable than the system based on PC, due to the variability of the mesencephalic angle. Coordinates are given in millimeters (mm) *Positive values* for X (lateral) are given to the right PPN as positive Y (anteroposterior) values are anterior to B point (point where the VLF meets a perpendicular *line* originated from Fastigium) and positive Z (rostrocaudal) values are rostral to B point. Relative to PC, rostral PPN is situated at 8.2 mm below PC (−8.2 mm) and caudal PPN at −14.2 mm for both sides. For comparison purposes, rostrocaudal values are also displayed in relation to PC. 15,430 μm slides contain the PPN, but 8 slides in 860 μm were chosen to demonstrate the histological localizations. They are named Plate 1 to Plate 8, increasing in number in the caudal-rostral direction. Plates 3–4, 5–6 and 7–8 are shown in Figs. 6, 7 and 8, respectively. The reference system adopted and overall location of plates within the brainstem is depicted in Fig. 9

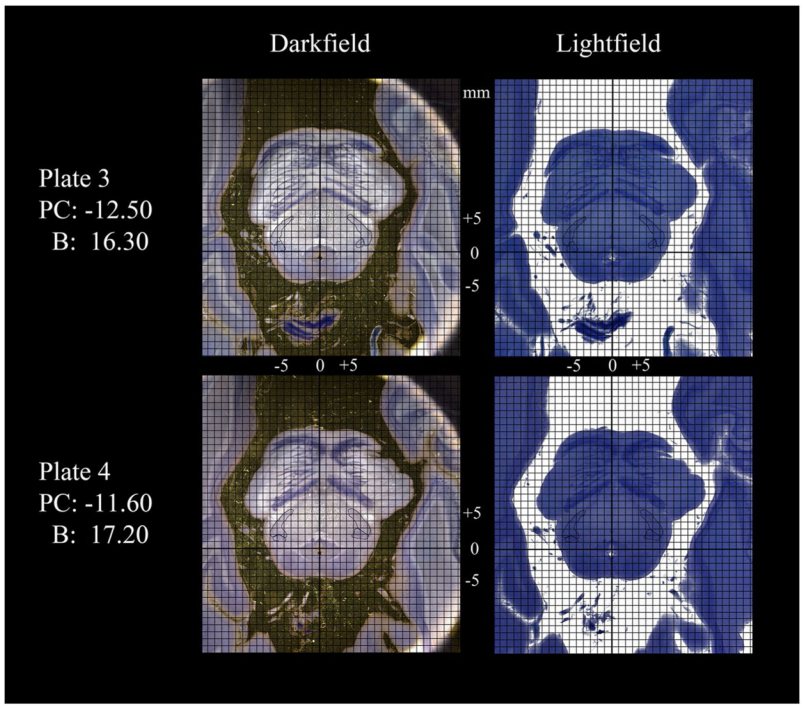

Fig. 7.
Plates 3–4. See Fig. 2 caption for details

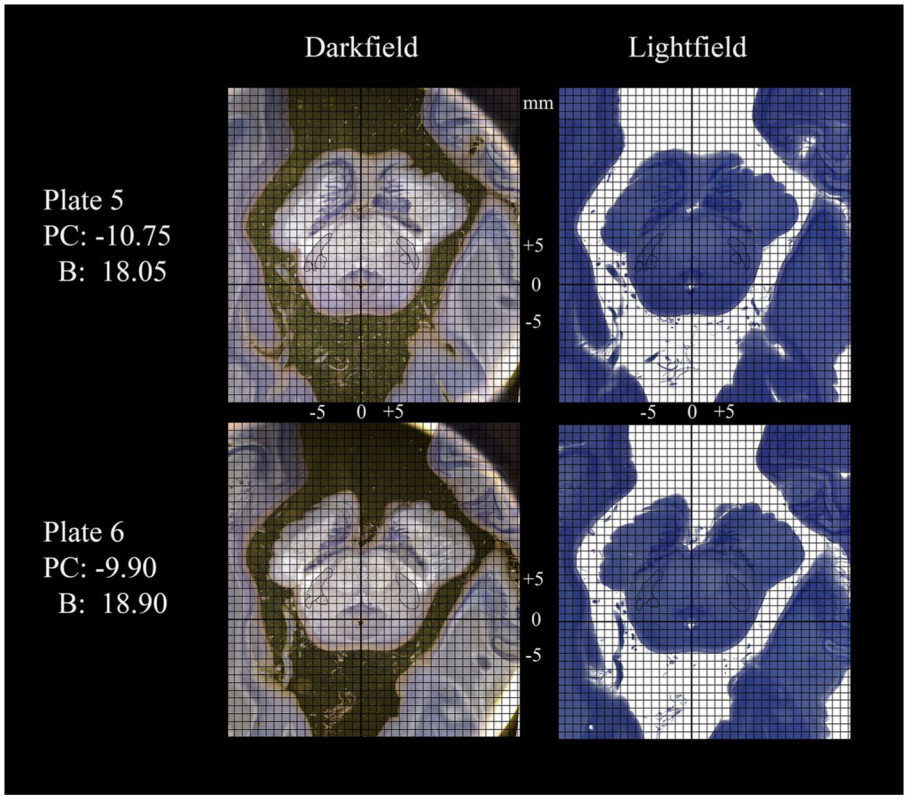

Fig. 8.
Plates 5–6. See Fig. 2 caption for details

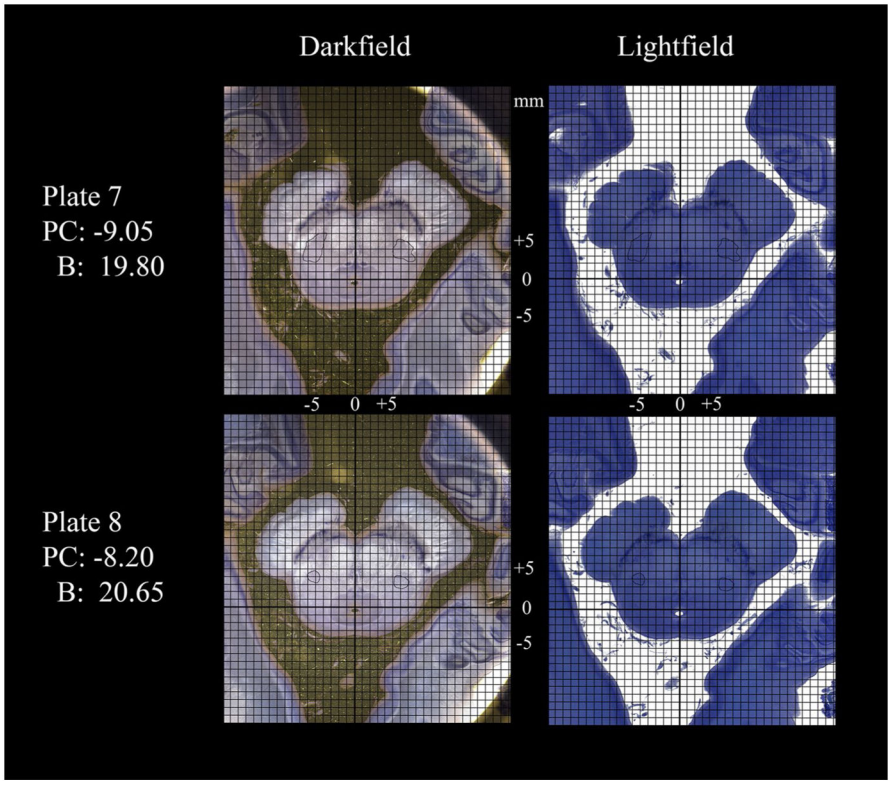

Fig. 9.
Plates 7–8. See Fig. 2 caption for details

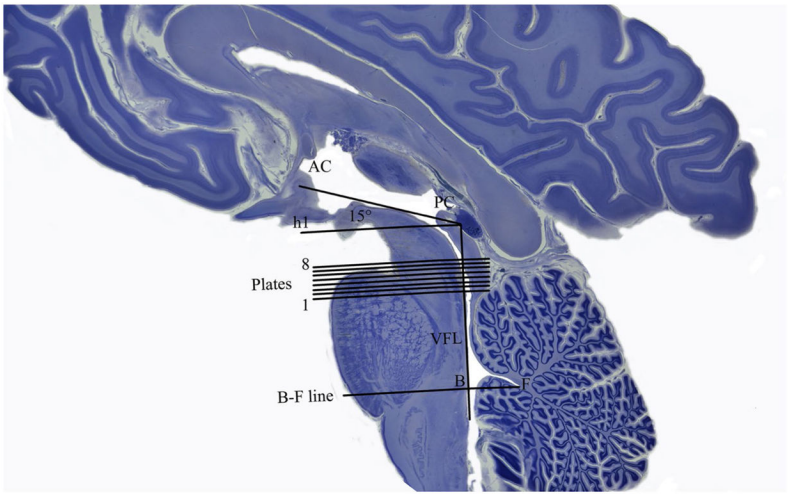

Fig. 10.

Reference System used for Figs. 2, 6, 7 and 8. See Fig. 2 caption for details

Table 1

Demographics of control volunteers

Case	Genre	Age
1	Female	21
2	Female	28
3	Male	43
4	Female	28
5	Female	26
6	Male	38
7	Male	66
8	Female	54
9	Female	21

Table 2

Stereotactic coordinates of the pedunculopontine nucleus relative to the posterior commissure (PC) and to B in Z axis (see Figs. 6, 7, 8, 9, 10)

	Right PPN	Left PPN
Rostrocaudal (Z)/mm		
Rostral		
PC	−8.20	−8.20
B	20.65	20.65
Caudal		
PC	−14.20	−14.20
B	14.6	14.6
Anteroposterior (Y)/mm		
Rostral	3.5	4.0
Caudal	2.0	1.5
Lateral (X)/mm		
Rostral	6.0	−5.5
Caudal	6.5	−6.0

*Negative values represent those inferior and to the left of PC

**Rostral = Plate 8, Caudal = Plate 1